Clinical Neurophysiology 131 (2020) 951–957

Contents lists available at ScienceDirect

Clinical Neurophysiology

journal homepage: www.elsevier.com/locate/clinph

Visualization of electrophysiological activity at the carpal tunnel area using magnetoneurography

Toru Sasaki [a], Shigenori Kawabata [b,*], Yuko Hoshino [b], Kensuke Sekihara [b], Yoshiaki Adachi [c], Miho Akaza [d], Isamu Ozaki [e], Koji Fujita [a], Akimoto Nimura [f], Toshitaka Yoshii [a], Yuki Miyano [g], Yuki Mitani [g], Taishi Watanabe [a,g], Shinji Sato [g], Sukchan Kim [g], Atsushi Okawa [a]

[a] Department of Orthopedic Surgery, Tokyo Medical and Dental University, 1-5-45 Yushima, Bunkyo-ku, Tokyo 113-8510, Japan
[b] Department of Advanced Technology in Medicine, Graduate School of Tokyo Medical and Dental University, 1-5-45 Yushima, Bunkyo-ku, Tokyo 113-8510, Japan
[c] Applied Electronics Laboratory, Kanazawa Institute of Technology, Kanazawa-shi, Ishikawa 920-1331, Japan
[d] Respiratory and Nervous System Science, Biomedical Laboratory Science, Graduate School of Tokyo Medical and Dental University, 1-5-45 Yushima, Bunkyo-ku, Tokyo 113-8510, Japan
[e] Faculty of Health Sciences, Aomori University of Health and Welfare, 58-1 Mase, Hamadate, Aomori-shi, Aomori 030-8505, Japan
[f] Department of Functional Joint Anatomy, Graduate School of Medical and Dental Sciences, Tokyo Medical and Dental University, 1-5-45, Yushima, Bunkyo-ku, Tokyo 113-8510, Japan
[g] Ricoh Institute of Future Technology, RICOH Company, Ltd., 2-3-10 Kandasurugadai Chiyoda-ku, Tokyo 101-0062, Japan

See Editorial, pages 938–939

ARTICLE INFO

Article history:
Accepted 14 November 2019
Available online 10 December 2019

Keywords:
Magnetoneurography
Evoked magnetic field
Carpal tunnel
Median nerve
Digital nerve
Conduction velocity

HIGHLIGHTS

- Neural activity in the carpal tunnel area can be visualized by magnetoneurography.
- Conductions due to stimulation of the index and middle digital nerves can be differentiated.
- Intra-axonal currents and currents flowing across the membrane can be visualized.

ABSTRACT

Objective: To establish a noninvasive method to measure the neuromagnetic fields of the median nerve at the carpal tunnel after electrical digital nerve stimulation and evaluate peripheral nerve function.
Methods: Using a vector-type biomagnetometer system with a superconducting quantum interference device, neuromagnetic fields at the carpal tunnel were recorded after electrical stimulation of the index or middle digital nerve in five healthy volunteers. A novel technique for removing stimulus-induced artifacts was applied, and current distributions were calculated using a spatial filter algorithm and superimposed on X-ray.
Results: A neuromagnetic field propagating from the palm to the carpal tunnel was observed in all participants. Current distributions estimated from the magnetic fields had five components: leading and trailing components parallel to the conduction pathway, outward current preceding the leading component, inward currents between the leading and trailing components, and outward current following the trailing component. The conduction velocity and peak latency of the inward current agreed well with those of sensory nerve action potentials.

Abbreviations: CSP, common-mode subspace projection; DIP, distal interphalangeal; MNG, magnetoneurography; MRI, magnetic resonance imaging; SNAP, sensory nerve action potential; SQUID, superconducting quantum interference device; UGRENS, unit gain constraint recursively applied null-steering spatial filtering.

* Corresponding author at: Department of Advanced Technology in Medicine, Graduate School of Tokyo Medical and Dental University, 1-5-45 Yushima, Bunkyo-ku, Tokyo 113-8510, Japan.

E-mail addresses: t-sasaki.orth@tmd.ac.jp (T. Sasaki), kawabata.orth@tmd.ac.jp (S. Kawabata), hoshino.atm@tmd.ac.jp (Y. Hoshino), k-sekihara@nifty.com (K. Sekihara), adachi@ael.kanazawa-it.ac.jp (Y. Adachi), mihonuro@tmd.ac.jp (M. Akaza), isamu@auhw.ac.jp (I. Ozaki), fujiorth@tmd.ac.jp (K. Fujita), nimura.orj@tmd.ac.jp (A. Nimura), yoshii.orth@tmd.ac.jp (T. Yoshii), yuki.yh.hasegawa@jp.ricoh.com (Y. Miyano), yuuki.ym.mitani@jp.ricoh.com (Y. Mitani), taishi.watanabe@jp.ricoh.com (T. Watanabe), shinji.s1.satoh@jp.ricoh.com (S. Sato), sukchan.kim@jp.ricoh.com (S. Kim), okawa.orth@tmd.ac.jp (A. Okawa).

https://doi.org/10.1016/j.clinph.2019.11.030
1388-2457/

Conclusion: Removing stimulus-induced artifacts enabled magnetoneurography to noninvasively visualize with high spatial resolution the electrophysiological neural activity from the palm to the carpal tunnel.

Significance: This is the first report of using magnetoneurography to visualize electrophysiological nerve activity at the palm and carpal tunnel.

1. Introduction

1.1. Electrophysiological examination of peripheral neuropathy

Carpal tunnel syndrome (CTS) is caused by entrapment of the median nerve at the wrist and is the most common nerve entrapment syndrome. Although CTS is diagnosed mainly from clinical findings, morphological evaluation by magnetic resonance imaging (MRI) (Razek et al., 2017) and ultrasound (Beekman and Visser, 2003) and functional evaluation by electrophysiological examination are performed as supplementary diagnostic tests. Despite advances in morphological evaluation technology with the development of MRI and ultrasound techniques, morphological evaluation alone is not sufficient for neurological functional evaluation. Electrophysiological examinations are useful to evaluate functionality and determine indications for surgical treatment, and there have been many reports of electrophysiological assessments for functional evaluation of CTS (Buchthal et al., 1974; Stevens, 1987; Jablecki et al., 1993). However, the conventional electrophysiological tests used to diagnose CTS, such as distal motor latency of the abductor pollicis brevis and digit-to-wrist antidromic sensory nerve conduction velocity, are associated with a high false-negative rate (Thomas et al., 1967; Sedal et al., 1973; Buchthal et al., 1974). This is because, when the conduction delay of a nerve lesion is short, it is difficult to detect an abnormality by measuring the conduction time of a much longer distance, as in the conventional method.

Inching methods are useful to diagnose focal conduction abnormalities at nerve entrapment sites. However, these methods have some disadvantages and are thus not used as a routine examination. Orthodromic inching methods require multiple recording surface electrodes and are time consuming (Seror, 1998), and the electric potential recording from the body surface is influenced by the presence of a thick skin or a thick transverse ligament (Werner and Andary, 2011). Antidromic inching methods sometimes struggle to determine the exact point of nerve activation due to the spread of the stimulating current (Kimura, 1979). The development is thus necessary of a non-technically demanding method that allows the detailed and rapid determination of the location and severity of peripheral nerve dysfunction.

1.2. Measurement of neuromagnetic fields

In contrast to surface electric potential measurement, the magnetic field is not affected by the surrounding tissue and has theoretically high spatial resolution (Trahms et al., 1989). Magnetic fields have been measured from the peripheral nerve of the upper extremities of humans (Trahms et al., 1989; Wikswo, 1990; Hoshiyama et al., 1999; Mackert, 2004; Nakanishi et al., 2004). However, there are no reports in the literature on magnetic field measurement of the palmar area from the body surface.

Our group has developed a technique to visualize the spatial distribution of the neural current of the peripheral nerve and spinal cord through neuromagnetic field measurement (Sato et al., 2009; Ishii et al., 2012; Sumiya et al., 2017; Ushio et al., 2019). With technical improvements, we have become able to visualize in a noninvasive manner and with high spatial resolution the distribution of neural currents, such as intra-axonal currents and volume currents including inward currents at depolarization sites. Although we had tried to measure the neuromagnetic field at the carpal tunnel after digital nerve stimulation, detection of the neuromagnetic field had been impossible due to the major artifact of the electrical stimulation applied to the finger, due to its close proximity to the recording site.

In this study, we combined a newly developed artifact removal method with magnetoneurography (MNG) from the body surface and report for the first time visualization of electrophysiological activity at the carpal tunnel area in response to digital nerve stimulation.

2. Methods

2.1. MNG system

All recordings were performed in a magnetically shielded room using a vector-type superconducting quantum interference device (SQUID) biomagnetometer system developed by Kanazawa Institute of Technology and RICOH Company, Ltd. (Adachi et al., 2017). The sensor array is composed of 44 SQUID magnetic flux sensors arranged at 20–25-mm intervals (Fig. 1a and b) along a cylindrical surface with a curvature radius of 200 mm. Each sensor is equipped with three pickup coils oriented orthogonally to one another to simultaneously detect magnetic field components both tangential and radial to the body surface. The SQUID sensor array is placed in a protrusion along the upper surface of the system. Seated subjects place their palm on the sensor area (Fig. 1c). The curved surface of the sensor area fits well to the shape of the human wrist joint and is more suitable for measuring the carpal tunnel magnetic field than the conventional flat sensor surface (Fig. 2b).

2.2. MNG measurement of the median nerve at the carpal tunnel area

All procedures in this study were approved by the Ethics Committee of Tokyo Medical and Dental University and were performed in accordance with the Declaration of Helsinki. We obtained written informed consent from all participants, who comprised five healthy volunteers aged 26–34 years (mean ± SD, 29.9 ± 3.0 years; one woman) without nervous system disease. Participants sat on a chair in a relaxed state and placed their palm on the sensor surface area with the forearm pronated. Lateral and frontal radiographs were taken to obtain positional information on the subject and the magnetic sensor. The index and middle finger were electrically stimulated at the distal interphalangeal (DIP) joint (square wave pulse; 3 Hz; 0.2 ms in duration). The index and middle finger were alternately stimulated at over 2–3 times the sensory threshold (intensity, 4.2–6.0 mA), and evoked magnetic fields were recorded at the surface of the palmar area using a 40-kHz sampling rate and 100–5000 Hz band-pass filter (Fig. 2a and b). For each finger, 2000 recordings of evoked magnetic fields were averaged.

To remove stimulus-induced artifacts from the acquired MNG signals, we also recorded the magnetic signal of the stimulus-

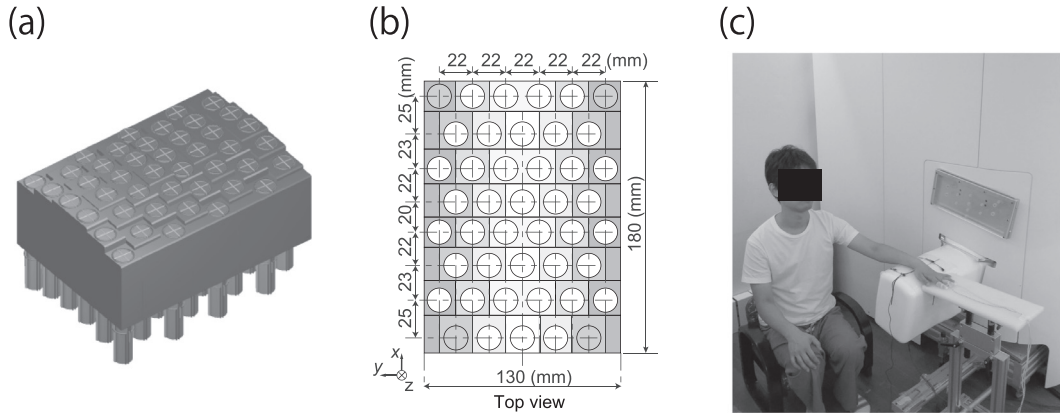

Fig. 1. Appearance and structure of the magnetoneurography (MNG) system. (a) The sensor array used to measure neuromagnetic fields. The array is composed of a 44-sensor vector-type SQUID biomagnetometer. The sensor surface is upward and slightly curved to fit the alignment of the limb joint. (b) The sensor arrangement. The 44 sensors are arranged in an area of 180 mm × 130 mm and spaced at 20–25-mm intervals. (c) MNG system and measurement position. The participant was seated on a chair in a relaxed state and placed their palm on the sensor area of the cryostat. © 2017 IEEE. Reprinted with permission from DOI:10.1109/TASC.2016.2631422.

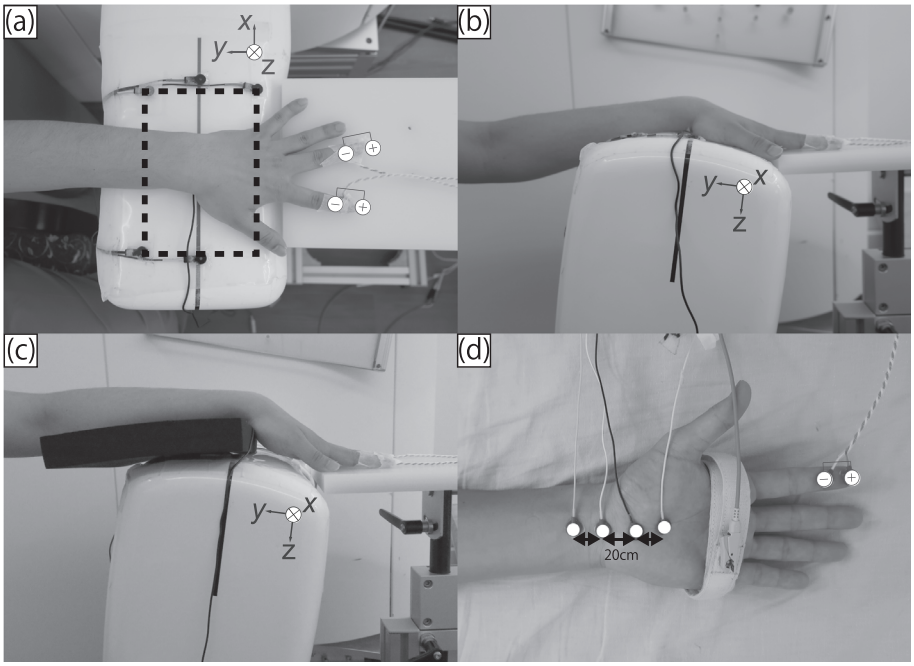

Fig. 2. Measurement of the neuromagnetic fields of the median nerve at the carpal tunnel area. (a) The subject put their carpal tunnel area on the center of the sensor area (dotted rectangle). We measured neuromagnetic fields in response to electrical stimulation of the digital nerve at the distal interphalangeal joint of the index or middle finger. (b) Side view of the measurement position. The sensor surface is slightly curved and fits the wrist joint. (c) Measurement of magnetic fields of stimulus-induced artifacts. A 30-mm urethane plate separates the nerve from the sensors and reduces the magnetic signal from neural activity. The position of the finger to be stimulated was the same. (d) Recording surface electrodes were placed at four locations—20 mm proximal and at 0, 20, and 40 mm distal to the wrist crease—and sensory nerve action potentials (SNAPs) were recorded in response to the index finger stimulation.

induced artifacts alone. A 30-mm urethane plate was placed between the palm and the sensor surface without moving the fingers to be stimulated, and the nerve magnetic field was measured under the same conditions (Fig. 2c). In this method, because the distance between the sensor and the nerve increases, the magnetic signals derived from the nerve are greatly reduced, allowing signals derived from the stimulus-induced artifacts alone to be acquired.

2.3. Measurement of sensory nerve action potentials

As a comparison with conventional electric potential recording, sensory nerve action potentials (SNAPs) were measured in all participants with orthodromic recording after stimulation of the index finger (Fig. 2d). The digital nerve was stimulated at the DIP joint of the index finger with orthodromic recording from the four points at the palm area (intensity, over twice the sensory threshold; frequency, 3 Hz). Recording surface electrodes were placed at four locations: 20 mm proximal and 0, 20, and 40 mm distal to the wrist crease.

2.4. Signal processing

First, we removed stimulus-induced artifacts from the acquired MNG signals by applying the common-mode subspace projection (CSP) algorithm (Watanabe et al., 2013). The CSP algorithm is used to calculate magnetic signals derived from neural activity alone using the entire magnetic signals (neural signal + artifact) and

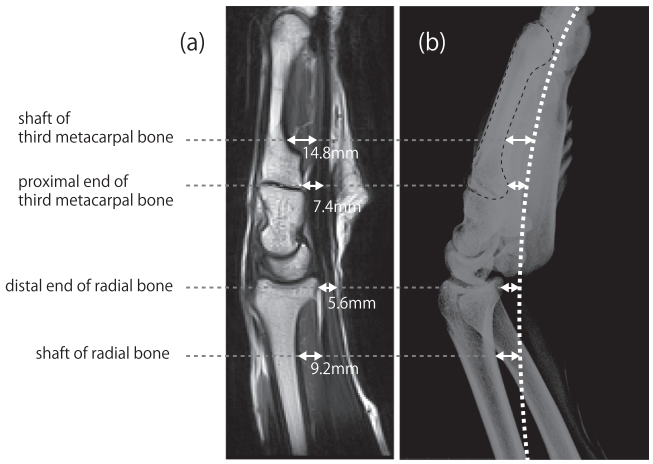

Fig. 3. Formulation of the depth between the nerve and the surface of the sensors. (a) These distances were chosen from the distance between the bone and nerve calculated from the MR images of five healthy volunteers. We measured distances at four points: the shaft of the radial bone, the distal radius, the base of the third metacarpal, and the shaft of the third metacarpal bone. The average distances were 9.2 mm, 5.6 mm, 7.4 mm, and 14.8 mm, respectively. (b) Lateral radiographs were taken to obtain positional information on the subject and the magnetic sensor. The distances from the MR images and the information from the X-ray images were used to define the region of interest (ROI).

the magnetic signal of the stimulus-induced artifacts alone. The CSP algorithm is effective when artifact sources are located in the vicinity of the signal source space.

A spatial filter algorithm, unit gain constraint recursively applied null-steering spatial filtering (UGRENS), was applied to the artifact-removed magnetic signal, and the temporal and spatial distributions of the currents were calculated at a region of interest (ROI) (Sekihara and Nagarajan, 2015). The ROI was at a depth of 9.2 mm from the palmar side of the shaft of the radial bone, 5.6 mm from the palmar side of the distal end of the radial bone, 7.4 mm from the palmar side of the base of the third metacarpal bone, and 14.8 mm from the palmar side of the shaft of the third metacarpal bone. These distances are the average distances between the bones and nerves measured from MRI of the five volunteers (Fig. 3). The calculated currents were superimposed on an X-ray image to visualize their distributions and intensities. Student's *t*-test was used to compare differences between the center of the second metacarpal bone and the calculated nerve route for the index finger stimulation and the middle finger stimulation. In this method, the current waveforms at arbitrary points in ROI can be calculated as if virtual electrodes were placed there. We set the virtual electrodes along the digital nerve and the median nerve at 10-mm intervals.

3. Results

3.1. Neuromagnetic field

The entire magnetic signal, comprising the neural signal and artifacts, extends from the palmar area to the carpal tunnel area in response to the digital nerve stimulation. The noise artifacts were too large to permit the identification of neural magnetic signals (Fig. 4a). After application of the CSP algorithm to the entire magnetic signal, small neural signals buried in the stimulus artifact were revealed in all volunteers (Fig. 4b and c).

Fig. 5 shows the evoked magnetic fields of a representative recording from the X-, Y-, and Z-directed coils (X, red; Y, green; Z, black; (b) index finger stimulation; (c) middle finger stimulation). The magnetic fields from the X- and Z-directed coils had biphasic waveforms and the magnetic fields from the Y-directed coil had triphasic waveforms, and these waveforms propagated in the distal to proximal direction. The averages of the maximum peak-to-peak amplitudes of the magnetic fields in each direction sensor were 78.4 ± 25.6 fT, 84.2 ± 28.2 fT, and 121.0 ± 21.3 fT (X, Y, and Z, respectively) in response to index finger stimulation and 86.0 ± 26.9 fT, 94.6 ± 27.0 fT, and 154.4 ± 32.3 fT (X, Y, and Z, respectively) in response to middle finger stimulation.

3.2. Current distribution

The current distributions calculated from the artifact-removed data using UGRENS were superimposed on an X-ray image of the hand as pseudocolor maps. We show a representative case in Fig. 6. At 2.1 ms after the index finger stimulation, the leading component, which comprises the currents running parallel to the nerve and was considered the intra-axonal current in our previous work (Fukuoka et al., 2002, 2004), appeared at the hook of hamate level and propagated from the carpal tunnel area in the proximal direction. At 3.3 ms after the stimulation, the trailing component appeared at the hook of hamate level. In addition, inward currents flowed perpendicularly between the leading and trailing components on both sides of the nerve. Moreover, outward currents were observed on both sides proximal to the intra-axonal leading component and distal to the trailing component. These inward and outward currents also propagated proximally along with the intra-axonal currents (Fig. 6a). There was a similar current pattern after middle finger stimulation (Fig. 6b). The calculated currents in response to the middle finger stimulation propagated along the

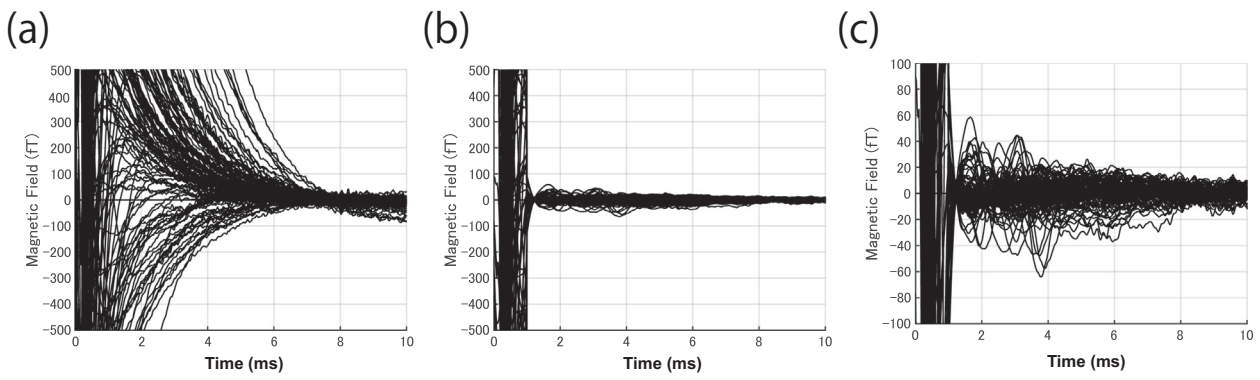

Fig. 4. Artifact removal by the common-mode subspace projection (CSP) algorithm. (a) The magnetic signals in response to index finger stimulation. We superimposed all magnetic fields measured at each sensor. (b) Artifact-removed signals after application of the common-mode subspace projection algorithm. Stimulus-induced artifacts were removed from the original signals. (c) The scale of the magnetic signal amplitude of Fig. 4b was expanded. Neural magnetic signals were clear.

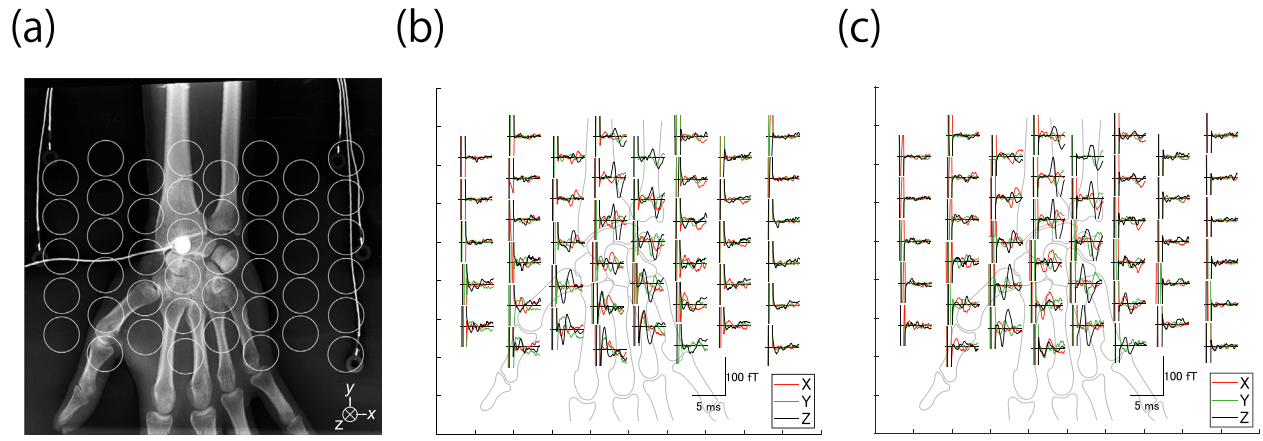

Fig. 5. Waveforms of the neural magnetic field at the palmar area in response to digital nerve stimulation. (a) An X-ray image of the hand superimposed on the positions of the sensors. (b) The three-directional magnetic signals recorded by each sensor after index finger stimulation. Viewed from the dorsal side of the hand, the sensor array was under the palmar side of the hand. Red traces are magnetic fields in the left–right direction (right is upward). Green traces are magnetic fields parallel to the nerve (proximal is upward). Black traces are magnetic fields in the volar–dorsal direction (volar is upward). (c) The magnetic signals after stimulation of the middle finger. The magnetic fields are illustrated as in (b). Red and black waveforms show biphasic waveforms and propagate in the distal to proximal direction. Green waveform shows triphasic waveforms.

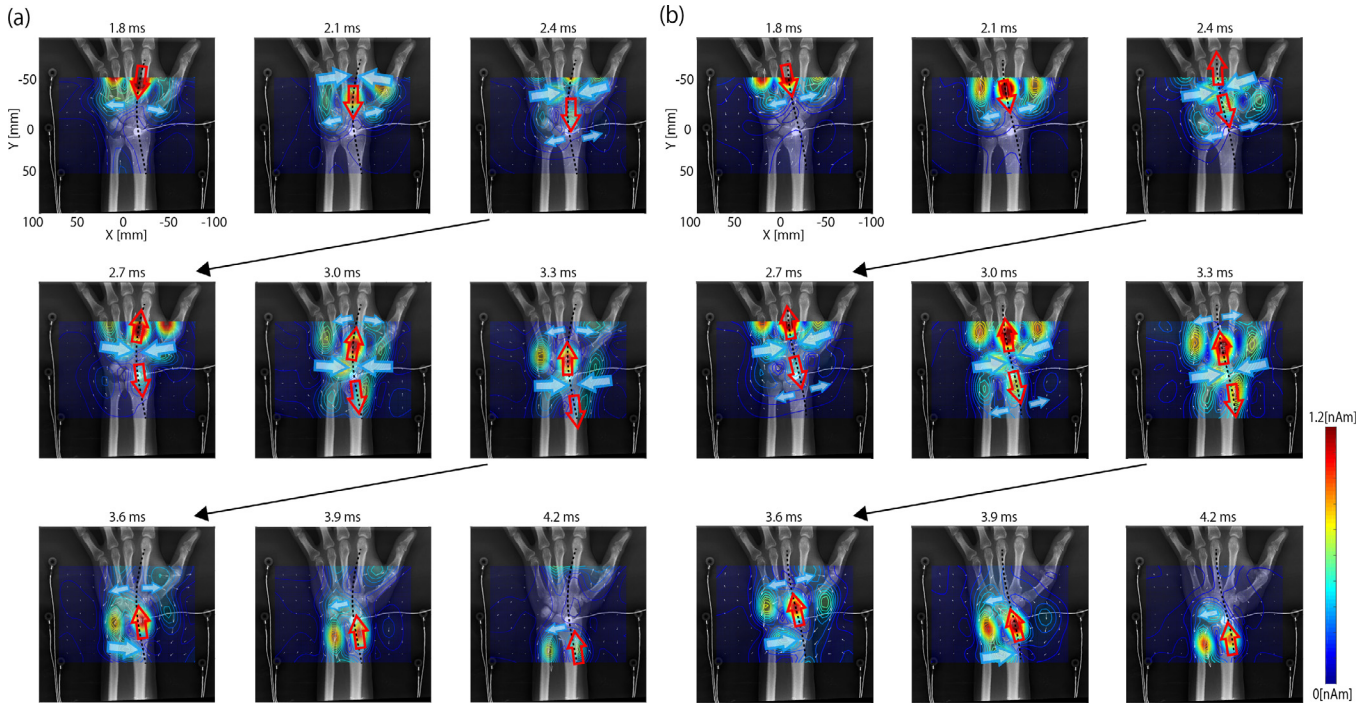

Fig. 6. Time course of the spatial distribution of calculated currents in a representative case. (a) Index finger stimulation. (b) Middle finger stimulation. Currents at the palmar area were calculated by UGRENS and superimposed on an X-ray image. The small white arrows indicate the direction of current at each position. Current intensity is shown by a color scale (red is higher). The leading component of the currents (downward-pointing red arrow) propagated proximally along the nerve, and the trailing component (upward-pointing red arrow) propagated later. Another component appeared on either side of the nerve and flowed perpendicularly between the leading and trailing components (inward-pointing blue arrows). In addition, two other outward components were observed prior to the leading component and posterior to the trailing component (outward-pointing blue arrows).

third metacarpal bone, which was ulnar (11.14 ± 5.7 mm ulnar at the mid-level of the metacarpal bone, $P = 0.012$) from the index finger stimulation currents, until the hook of hamate level. Proximal to the hook of hamate level, currents in response to the middle finger stimulation propagated along the same pathway as the index finger stimulation currents.

3.3. Waveforms of the calculated currents at the virtual electrodes

We set the virtual electrodes along the nerve pathway and calculated the waveforms of the currents parallel to the conduction pathway (Fig. 7b). In addition, the waveforms of the currents perpendicular to the conduction pathway were calculated at each virtual electrode, which was set 15 mm ulnar from the conduction pathway (Fig. 7a). The upward peak in the waveform of the currents parallel to the conduction pathway is equivalent to the leading component in Fig. 6a, and the downward peak is equivalent to the trailing component (Fig. 7b). The waveform of the currents perpendicular to the conduction pathway had three phasic waveforms (Fig. 7a). The first downward peak, the second upward peak, and the third downward peak correspond to the outward current preceding the intra-axonal leading component, the inward currents

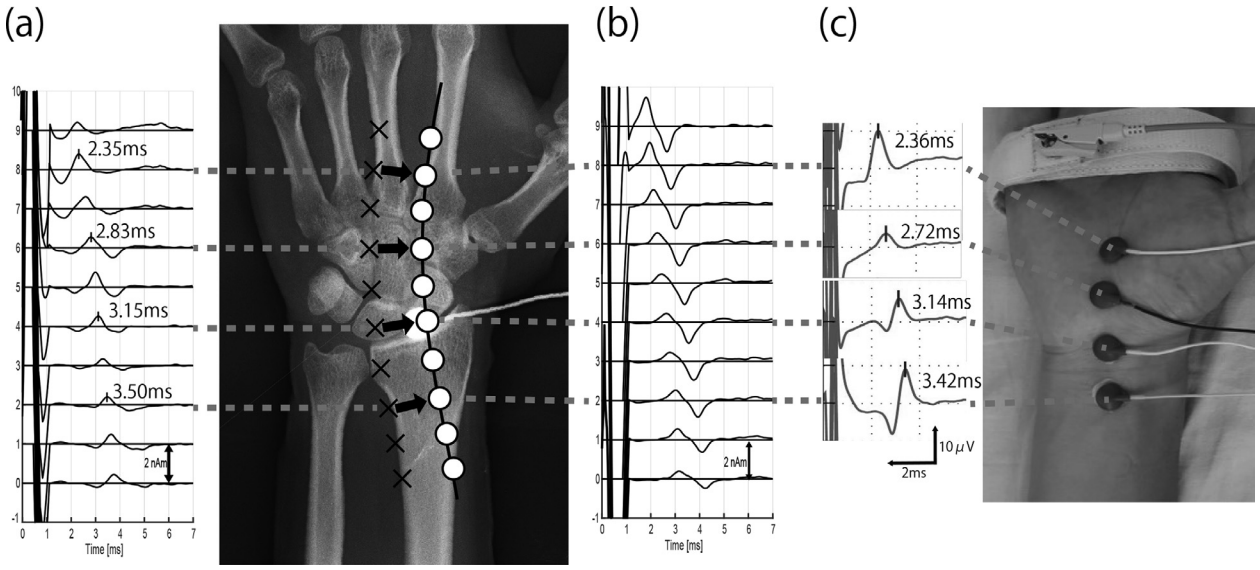

Fig. 7. Waveforms of calculated currents at the "virtual electrodes" and sensory nerve action potentials (SNAPs) in response to the index finger stimulation. (a) Currents at virtual electrodes (X mark) 15 mm lateral from the nerve pathway (upward is toward the nerve pathway). (b) Currents at virtual electrodes (white circle) along the nerve pathway (the distal to proximal direction is upward). (c) Sensory nerve action potentials with orthodromic recording.

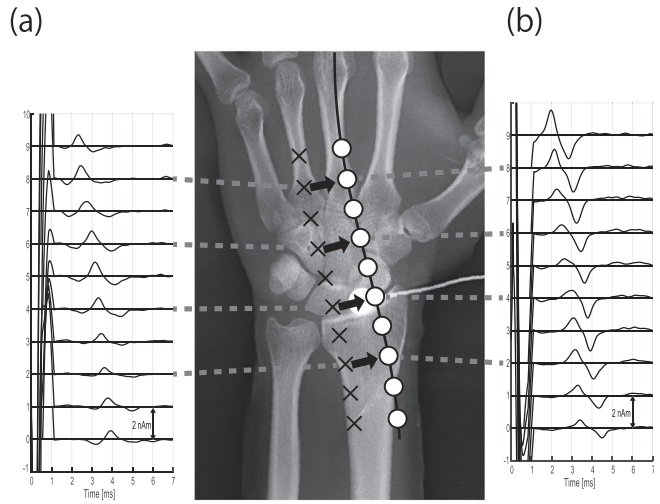

Fig. 8. Waveforms of calculated currents at the "virtual electrodes" in response to the middle finger stimulation. Currents are illustrated in a similar manner to Fig. 7. (a) Currents at virtual electrodes (X mark) 15 mm lateral from the nerve pathway (upward is toward the nerve pathway). (b) Currents at virtual electrodes (white circle) along the nerve pathway (the distal to proximal direction is upward).

between the leading and trailing components, and the outward current following the intra-axonal trailing component in Fig. 6a, respectively. The calculated waveform after the middle finger stimulation showed the same pattern as the index finger stimulation (Fig. 8). The currents parallel and perpendicular to the conduction pathway were propagated in the distal to proximal direction in both the index and middle finger stimulations.

From the currents flowing perpendicularly to the conduction pathway, we calculated the maximum current value at the center of the carpal tunnel area (the midline between the hook of hamate bone and the pisiform bone). The averages of the maximum current values of the five hands were 0.34 ± 0.08 nAm in response to the index finger stimulation and 0.55 ± 0.43 nAm in response to the middle finger stimulation. The average conduction velocities calculated from the peak latency of the inward currents were 52. 6 ± 4.6 m/s (index finger) and 52.7 ± 3.5 m/s (middle finger).

3.4. Comparison of the calculated currents and SNAPs

We compared the calculated current waveform with the SNAP waveform in response to the index finger stimulation. In all five cases, there was almost a perfect match between the peak latencies of the inward current flowing perpendicularly to the conduction pathway of the virtual electrode set at the same level as the recording electrode of SNAPs (Fig. 7a) and the negative peak latencies of SNAP (Fig. 7c). The average conduction velocity calculated from the peak latency of the SNAPs was 52.7 ± 3.5 m/s.

4. Discussion

In this study, the CSP algorithm removed stimulus-induced artifacts and enabled very early neuronal signals buried in stimulus-induced artifacts to be visualized. The current calculated from the artifact-removed signal comprised five current components. The leading components and trailing components parallel to the conduction pathway, the outward current preceding the leading component, the inward currents between the leading and trailing components, and the outward current following the trailing component are considered to respectively indicate the intra-axonal leading current, the intra-axonal trailing current, the outward current generated from the membrane capacity current, the inward sodium current resulting from depolarization, and the outward current generated from the repolarization phase (Noble, 1966). These currents showed characteristics of axonal activity, and the currents superimposed on the X-ray image were conducted along the nerve pathway from the digital nerve to the median nerve. The conduction pathway was displaced to the radial side at the forearm due to its pronation. Compared with SNAPs, the peak latency of the inward current and the negative latency of SNAPs matched, and the conduction velocity was almost the same.

From these results, we consider that we were able, for the first time, to detect neural magnetic signals by using the CSP method and to visualize the current distribution derived from the axonal activity around the carpal tunnel area. We found that MNG has sufficiently high spatial resolution to distinguish the digital nerve activities of the middle and index fingers.

Fukuoka et al. (2004); (Tomori et al., 2010) reported that MNG could identify the conduction block site with high spatial resolu-

tion in animal experiments. MNG may be able to reduce the false-negative rate of electrophysiological testing in carpal tunnel syndrome through diagnosis of the local conduction block, which is difficult to detect by the conventional method. From the viewpoint of a surgeon, superimposition of the conduction block site and morphological information, such as that provided by a plain X-ray or MR image, might be useful for surgical planning.

In addition, MNG might be able to visualize not only the currents flowing across the membrane (outward current generated from the membrane capacity current, inward sodium current resulting from depolarization, and outward current generated from the repolarization phase), but also leading and trailing intra-axonal currents, which cannot be evaluated by the conventional electrical potential measurement. Thus far, it is unclear how the intra-axonal currents change in pathological situations such as entrapment neuropathy, but we plan to prove the clinical significance of the intra-axonal currents by accumulating MNG data on patients in the future.

5. Conclusion

We succeeded in using MNG to noninvasively visualize electrophysiological activity at the palmar area, the carpal tunnel area, and the wrist in response to digital nerve stimulation. Technical improvements comprising the removal of stimulus-induced artifacts and source analysis allowed us to calculate the current waveform at an arbitrary point and superimpose the nerve action currents on morphological information such as X-ray images with high spatial resolution. For the axonal activity, MNG was able to visualize the intra-axonal currents and the currents flowing across the membrane. This system will become a novel method for evaluating peripheral nerve function and contribute to the diagnosis of various peripheral neuropathies, as well as carpal tunnel syndrome.

Funding

This research was supported by the RICOH Company Grand Number 1250000125012A210. The funding body played no role in study design, data collection and analysis, preparation of the manuscript, or the decision to publish.

CRediT authorship contribution statement

Toru Sasaki: Data curation, Formal anlysis, Investigation, Methodology, Resources, Writing - original draft. **Shigenori Kawabata:** Funding acquisition, Methodology, Project administration, Writing - review & editing. **Yuko Hoshino:** Formal anlysis, Methodology. **Kensuke Sekihara:** Formal anlysis, Visualization. **Yoshiaki Adachi:** Validation, Writing - original draft. **Miho Akaza:** Data curation, Formal analysis, Investigation, Methodology. **Isamu Ozaki:** Methodology, Supervision, Validation, Writing - original draft. **Koji Fujita:** Conceptualization, Methodology. **Akimoto Nimura:** Conceptualization, Methodology. **Toshitaka Yoshii:** Conceptualization, Methodology. **Yuki Miyano:** Data curation, Formal analysis, Investigation, Software. **Yuki Mitani:** Data curation, Formal analysis, Investigation, Software. **Taishi Watanabe:** Data curation, Formal analysis, Investigation, Software. **Shinji Sato:** Data curation, Formal analysis, Investigation, Software. **Sukchan Kim:** Data curation, Formal analysis, Investigation, Software. **Atsushi Okawa:** Project administration, Supervision.

Declaration of Competing Interest

The authors declare that they have no known competing financial interests or personal relationships that could have appeared to influence the work reported in this paper.

References

Adachi Y, Kawabata S, Fujihira J, Uehara G. Multi-channel SQUID magnetospinogram system with closed-cycle helium recondensing. IEEE Trans Appl Supercond 2017;27.
Beekman R, Visser LH. Sonography in the diagnosis of carpal tunnel syndrome: a critical review of the literature. Muscle Nerve 2003;27:26–33.
Buchthal F, Rosenfalck A, Trojaborg W. Electrophysiological findings in entrapment of the median nerve at wrist and elbow. J Neurol Neurosurg Psychiatry 1974;37:340–60.
Fukuoka Y, Komori H, Kawabata S, Ohkubo H, Shinomiya K. Visualization of incomplete conduction block by neuromagnetic recording. Clin Neurophysiol 2004;115:2113–22.
Fukuoka Y, Komori H, Kawabata S, Ohkubo H, Shinomiya K, Terasaki O. Imaging of neural conduction block by neuromagnetic recording. Clin Neurophysiol 2002;113:1985–92.
Hoshiyama M, Kakigi R, Nagata O. Peripheral nerve conduction recorded by a micro gradiometer system (micro-SQUID) in humans. Neurosci Lett 1999;272:199–202.
Ishii S, Kawabata S, Tomizawa S, Tomori M, Sakaki K, Shinomiya K, et al. Conductive neuromagnetic fields in the lumbar spinal canal. Clin Neurophysiol 2012;123:1656–61.
Jablecki CK, Andary MT, So YT, Wilkins DE, Williams FH. Literature review of the usefulness of nerve conduction studies and electromyography for the evaluation of patients with carpal tunnel syndrome. AAEM Quality Assurance Committee Muscle Nerve 1993;16:1392–414.
Kimura J. The carpal tunnel syndrome: localization of conduction abnormalities within the distal segment of the median nerve. Brain 1979;102:619–35.
Mackert BM. Magnetoneurography: theory and application to peripheral nerve disorders. Clin Neurophysiol 2004;115:2667–76.
Nakanishi K, Mashiko T, Fujimoto Y, Tanaka N, Iwase Y, Ishida O, et al. Wide-range visualization of compound nerve action magnetic fields in the human median and ulnar nerves from the forearm to Erb's point. Neurosci Lett 2004;356:151–3.
Noble D. Applications of Hodgkin-Huxley equations to excitable tissues. Physiol Rev 1966;46:1–50.
Razek AAKA, Shabana AA, El Saied TO, Alrefey N. Diffusion tensor imaging of mild-moderate carpal tunnel syndrome: correlation with nerve conduction study and clinical tests. Clin Rheumatol 2017;36:2319–24.
Sato T, Adachi Y, Tomori M, Ishii S, Kawabata S, Sekihara K. Functional Imaging of Spinal Cord Electrical Activity From Its Evoked Magnetic Field. IEEE Trans Biomed Eng 2009;56:2452–60.
Sedal L, McLeod JG, Walsh JC. Ulnar nerve lesions associated with the carpal tunnel syndrome. J Neurol Neurosurg Psychiatry 1973;36:118–23.
Sekihara K, Nagarajan SS. Electromagnetic Brain Imaging. Cham: Springer International Publishing; 2015.
Seror P. Orthodromic inching test in mild carpal tunnel syndrome. Muscle Nerve 1998;21:1206–8.
Stevens JC. AAEE minimonograph #26: The electrodiagnosis of carpal tunnel syndrome. Muscle Nerve 1987;10:99–113.
Sumiya S, Kawabata S, Hoshino Y, Adachi Y, Sekihara K, Tomizawa S, et al. Magnetospinography visualizes electrophysiological activity in the cervical spinal cord. Sci Rep 2017;7:2192.
Thomas JE, Lambert EH, Cseuz KA. Electrodiagnostic aspects of the carpal tunnel syndrome. Arch Neurol 1967;16:635–41.
Tomori M, Kawabata S, Tomizawa S, ishii S, Enomoto M, et al. Diagnosis of incomplete conduction block of spinal cord from skin surface using spinal cord evoked magnetic fields. J Orthopaedic Science 2010;15(3):371–80. https://doi.org/10.1007/s00776-010-1463-3. In press.
Trahms L, Erne SN, Trontelj Z, Curio G, Aust P. Biomagnetic functional localization of a peripheral nerve in man. Biophys J 1989;55:1145–53.
Ushio S, Hoshino Y, Kawabata S, Adachi Y, Sekihara K, Sumiya S, et al. Visualization of the electrical activity of the cauda equina using a magnetospinography system in healthy subjects. Clin Neurophysiol 2019;130:1–11.
Watanabe TKY, Ukegawa D, Kawabata S, Adachi Y, Sekihara K. Removal of stimulus-induced artifacts in functional spinal cord imaging. 2013 35th Annual International Conference of the IEEE Engineering in Medicine and Biology Society (EMBC), 2013.
Werner RA, Andary M. Electrodiagnostic evaluation of carpal tunnel syndrome. Muscle Nerve 2011;44:597–607.
Wikswo JP. Intraoperative Recording of the Magnetic Field of a Human Nerve. Advances in Biomagnetism. Springer; 1990. p. 137–40.